Multi-Frequency Microwave Imaging Inspection for Industrial Food Quality Assessment

Multi-frequency Microwave Imaging Inspection for Industrial Food Quality Assessment

Calin Ion Maraloiu*, Jorge Alberto Tobon Vasquez†, Marco Ricci†, Lorenzo Crocco§, Francesca Vipiana*
*Department of Electronics and Telecommunications, Politecnico di Torino, 10129 Torino, Italy, calin.maraloiu@polito.it
†Wavision S.r.l., 10129 Torino, Italy, marco.ricci@wavision.it
§CNR-IREA, National Research Council, Napoli, Italy, crocco.l@irea.cnr.it

***Abstract*—Progressive automation and throughput scaling are essential for the economic development and robustness of a productive food manufacturing company. Reliable scanning verification technologies must be put in place to ensure products quality and conformity. Due to the impressive yield of high-speed production lines, possible and undesirable malfunctionings may irreversibly alter the compliance of some of the fabricated samples, by contaminating them with foreign intrusions. In this paper, we propose the use of microwave imaging as a novel exploitable strategy, complementary to other well-established technologies (such as X-rays and metal detectors), to sense foreign intrusions inside food products. The examined setup is made of a set of printed monopole antennas mounted on a 3D printed arch, which suits the placement on production chain conveyor belts. Foreign body reconstructions for an oil-filled jar, scanned in a fixed position, have been obtained in the frequency range $9-10$ GHz. The impact of mathematical multi-frequency approaches is explored, combining available information from different spectral perspectives.**

***Index Terms*—microwave antennas, microwave imaging, multi-frequency, non-destructive testing.**

I. Introduction

Contaminated products with foreign intrusions statistically represent a very modest percentage of the annual food and beverage industrial production. Nevertheless, even such a small amount is sufficient to undermine the trustworthy reputation of manufacturing companies, leading to severe consequences for the costs related to batch recalls and loss of customers trust. At European level, the Rapid Alert System for Food and Feed (RASFF) is the food safety standard exploited to monitor and classify product non-compliance in the food-processing industry among the member countries [1].

To assess the absence of fragments, it is mandatory to perform rapid individual verifications of the samples, with the aid of effective scanning technologies, to preventively discard the defective ones from the production chain. Imaging technologies such as X-rays machines and metal detectors are currently deployed for this purpose. However, their intrinsic limitations in detecting some specific materials, such as low density plastics for X-rays and any non-metallic material for metal detectors, may not fully prevent the issue.

In the recent years, microwave imaging (MWI) technology has been considered to overcome these limitations [2] and perform the monitoring task by producing an image [3], [4] or performing an automated classification [5]. MWI shares some features with the commonly exploited inspection techniques like rapid processing, non-invasivity and non-destructivity. On the other hand, MWI devices add up several advantages such as compactness, portability, low-maintenance and low-cost in terms of energetic consumption. Additionally, they do not require specific training for factory workers or protection protocols, since only harmless non-ionizing electromagnetic radiations are involved. Exploiting the antennas both as transmitters and receivers, the MWI purpose is to obtain 3D dielectric contrast reconstruction maps. Contaminants, due to different dielectric permittivity characteristics with respect to the object content, alter the incident electromagnetic signal and this translates into useful information for the object contrast mapping.

One of the main challenges to be faced when designing an MWI device for quality inspection of products in food industry is the need of performing the monitoring task without interrupting the production chain. To this end, it is necessary to keep the overall measurement time compatible with the speed of the conveyor belt [2], [3]. This results in an upper bound on the number of spatial acquisitions which can be performed and henceforth on the number of antennas.

In this paper, we investigate the use of the received signals at different frequencies via a MWI inspection system: this is a key point to success in properly inspecting and reconstructing a contrast image of the product under analysis. For this purpose, three possible approaches to process and combine data acquired at multiple frequencies are presented and assessed with experimental data of a jar full of oil, whose position is fixed with respect to the setup.

II. Microwave imaging problem and multi-frequency methods

A. Problem formulation

As discussed in [2], [3], the imaging problem underlying the application at hand can be modelled in terms of a linearized inverse problem. Using a compact notation, and considering a single frequency, such an inverse problem can be cast as:

$$\Delta S(\mathbf{r}_p, \mathbf{r}_q) = \mathcal{L}\{\Delta\chi\}, \tag{1}$$

where $\mathbf{r}_p, \mathbf{r}_q$ are the vector positions of respectively the transmitting and receiving antennas. $\Delta\chi$ is the normalized

dielectric unknown contrast between the contaminant and the host medium, defined as:

$$\Delta\chi(\mathbf{r}) = \frac{\epsilon(\mathbf{r}) - \epsilon_b}{\epsilon_b}, \tag{2}$$

where $\epsilon(\mathbf{r})$ is the spatial relative dielectric permittivity of the domain under analysis with respect to the position $\mathbf{r}$, and ϵ_b is the relative dielectric permittivity of the reference material (in this case oil). ΔS is the differential scattering matrix and represents the data of the problem. It is obtained as the difference between the scattering matrix measured at the antennas ports S_c during operation and the scattering matrix of the reference contaminant-free object S_r.

The continuous problem cast in (1) is spatially discretized. To this end the discrete counterpart of $\mathcal{L}$, say $[L]$, is numerically computed. In this paper, we use a finite element method (FEM) approach [6]. The discretized problem takes the following matrix-form:

$$[\Delta S] = [L][\Delta\chi], \tag{3}$$

where the vector $[\Delta S]$ is the column-wise reshaped differential scattering matrix and has size N, which corresponds to the number of entries of the scattering matrix. Finally, the truncated singular value decomposition (TSVD) method is applied to (3) to retrieve the dielectric contrast $[\Delta\chi]$.

B. Multi-frequency approaches

In order to seamlessly integrate the MWI device within the production chain, it is important to build a setup that is compliant with the industrial plant processing constraints, such as acquisition process and conveyor belt speed. This introduces some limitations in the obtainable spatial sampling, directly linked to the number of placeable antennas.

On the other hand, increasing the amount of independent data is important to improve the quality of the achieved reconstructions both in terms of rejection of the unavoidable presence of noise on data and minimization of artifacts in the obtained images. Within the above mentioned constraints, this goal can be achieved considering multi-frequency data instead of single frequency data as done so far [3], [4].

In the following, three possible approaches to combine information from F different frequencies are described.

1) Contrast product: The first method consists in multiplying the F dielectric contrasts $[\Delta\chi]_f$, obtained at each frequency, re-normalizing the result with respect to the maximum of the product. This corresponds to perform an intersection of the different frequency maps:

$$[\Delta\chi^{\mathrm{P}}] = \frac{\prod_{f=1}^{F}[\Delta\chi]_f}{\max\prod_{f=1}^{F}[\Delta\chi]_f}. \tag{4}$$

2) Contrast average: The second approach consists in summing the F dielectric contrasts $[\Delta\chi]_f$ obtained by solving (3) at each frequency, and normalizing the obtained sum with its maximum. This corresponds to the average of the single frequency maps:

$$[\Delta\chi^{\mathrm{S}}] = \frac{\sum_{f=1}^{F}[\Delta\chi]_f}{\max\sum_{f=1}^{F}[\Delta\chi]_f}. \tag{5}$$

3) Multi-frequency operator inversion: The third approach processes all the available multi-frequency data simultaneously, assuming that the dispersivity of the involved material can be neglected. Accordingly, this corresponds to augment by a frequency factor F the row-dimension of the original matrix, merging into a single multi-frequency $[L^F]$ operator all the single-frequency $[L_f]$ ones. Consequently, the data are rearranged increasing by the frequency factor the N size column vector $[\Delta S^F]$, whereas, owing to the non-dispersive assumption, the dielectric contrast $[\Delta\chi^M]$ of the multi-operator problem is unchanged and still encoded in an M elements column vector. The problem takes the following block matrix shape:

$$[\Delta S^F] = [L^F][\Delta\chi^M], \tag{6}$$

where $[\Delta S^F] = [\Delta S_1\ \Delta S_2 ...\ \Delta S_f ...\ \Delta S_F]^T$ and $[L^F] = [L_1\ L_2 ...\ L_f ...\ L_F]$. It is important to notice that the simultaneous processing of the multiple frequency data performed in the third approach does not entail an increase of the computational burden of the image formation. This task is still performed in real-time, since the intensive part of the inversion task (i.e., the construction of the matrix $[L^F]$ and the computation of its SVD) is carried out off-line only once.

III. Microwave imaging setup and experimental results

The system used to perform the experiments to validate the approaches described in the previous section is shown in Fig. 1. The setup consists of a set of six printed monopole antennas [7], working as both transmitters and receivers. The antennas are placed on 3D printed support having the form of an arch, surrounding the analyzed domain (shielded from any outcoming electromagnetic disturbances). A six-port vector network analyzer (VNA) [8] and a computer are employed for the measurement chain unit and post-processing core, to allow the appropriate switching process among the antennas and to provide the required scattering matrices.

The analyzed product is a jar full of oil. The choice of this medium lies in its transparency, allowing for an easy

TABLE I
Measured values of relative electric permittivity and conductivity

sunflower seed oil	ϵ_r	σ (S/m)
9.00 GHz	2.565	0.159
9.25 GHz	2.503	0.175
9.50 GHz	2.490	0.189
9.75 GHz	2.515	0.205
10.00 GHz	2.538	0.234

Fig. 1. Setup configuration: the antennas are placed around an arch surrounding the conveyor belt and the setup is shielded from any external electromagnetic disturbances. A black rubber fragment is placed in the left-medium part of the jar to contaminate the scenario.

visual inspection of the product. To build the $[L]$-operators, the materials must be first measured and characterized along the frequency range in terms of dielectric properties, as shown in Table I, through a probe [9]. The contaminant is a rubber fragment and is introduced through a sub-mm nylon wire, allowing for an accurate positioning. In all the following images, showing the reconstructed dielectric contrast inside the jar, a small black sphere is placed to easily identify the expected position of the contaminant, to replicate the scenario in Fig. 1. The choice of the operating frequency range is carried out accounting the trade-off between achievable spatial resolution in the imaging results and the depth at which the probing wave can penetrate the inspected item. In particular, higher frequencies improve the spatial resolution but reduce the penetration depth. Considering the size of the inclusion and the oil content (that has lower attenuation compared to water), the $9-10\,\mathrm{GHz}$ frequency range has been selected in this study. Assuming a $0.25\,\mathrm{GHz}$ frequency step, five $[L]$-operators are built within the considered range and exploited to perform both single frequency imaging and multi-frequency imaging using the three approaches described above. Finally, to simplify the readability of the imaging results, the TSVD retrieved contrast image is turned into a binarized image. The applied binarization threshold is set forcing to 0 all locations where the value of the retrieved normalized contrast is lower than 85%.

Fig. 2 reports the reconstructions achieved when separately processing the data at each frequency. We can observe that all images match the expected position of the inclusion. However, the presence of artifacts in all cases can make the result difficult to understand.

Fig. 3 shows the results obtained with the three considered multi-frequencies approaches. As can be immediately noticed, whatever the approach, combining the patterns allows to focus

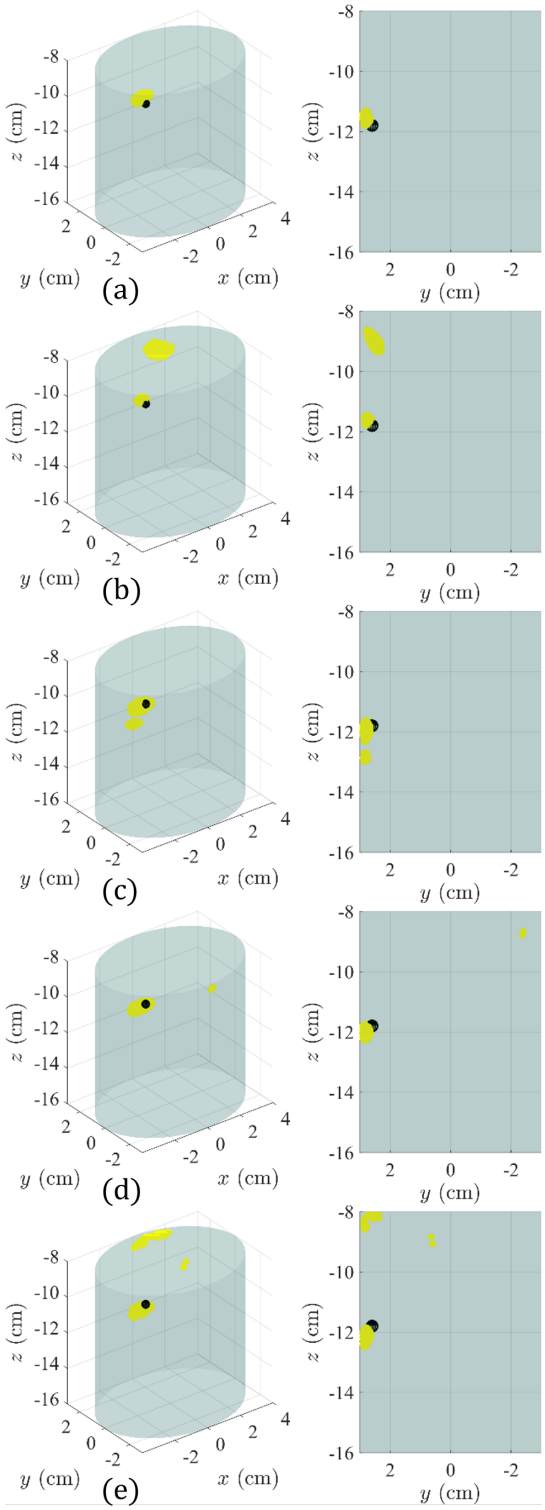

Fig. 2. Single-frequency dielectric contrast reconstruction maps in the range from 9 GHz (a) to 10 GHz (e) with an intermediate step of 0.25 GHz (b-c-d).

the proper location of the intrusion and filter out the artifacts. In particular, as expected, the image product (Fig. 3.(a)) gives back the most selective result, whereas image average (Fig. 3.(b)) blurs the contrast region, leading to a larger spot. Finally,

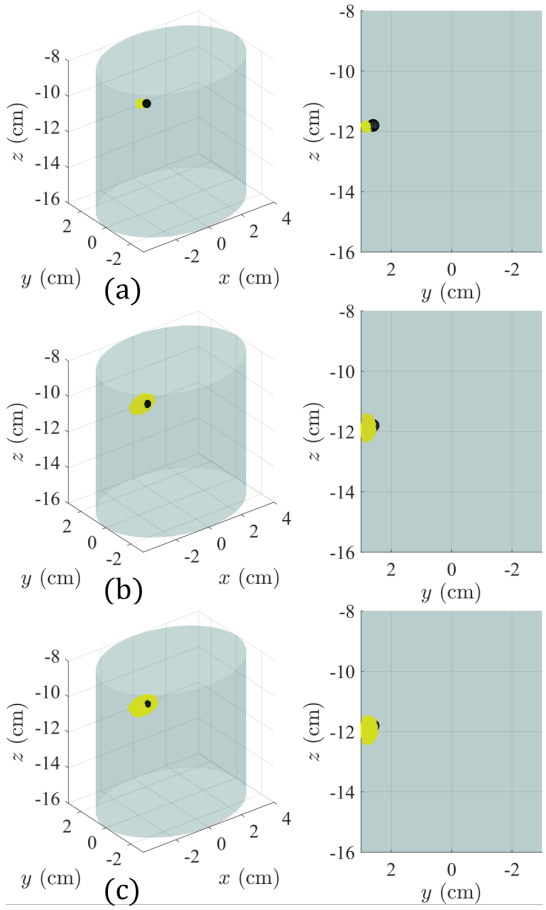

Fig. 3. Multi-frequency images: the single-frequency information shown in Fig. 2 is processed to obtained the contrast product (a), the contrast sum (b) and the multi-operator image (c).

the multi-frequency operator inversion is shown in Fig. 3.(c). Also in this case, artifacts are properly filtered.

To assess the best achievable reconstructions the binarized projection of the expected unknown contrast function on the TSVD basis functions has been considered (Fig. 4). The expected unknown contrast is built assigning to the region of interest the highest value of the normalized dielectric contrast.

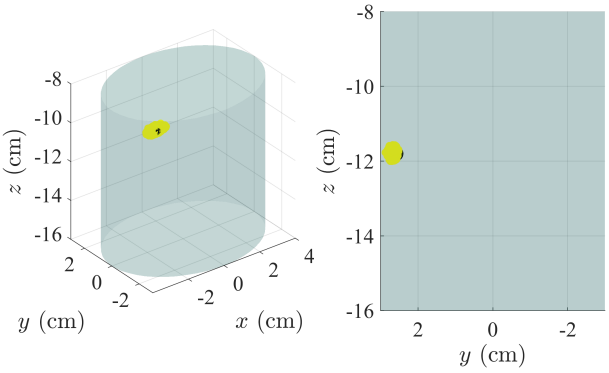

Fig. 4. Projection of the multi-operator (6) on the targeted location.

As can be seen, the obtained results (Fig. 3.(c)) are very similar to the ideal reconstruction (Fig. 4).

IV. Conclusion and Perspectives

In this paper, we presented a multi-frequency methodology to improve the quality of the dielectric mapping reconstructions, fading out noisy side effects, in the use of the MWI technology for the inspection of foreign contamination in food products.

Further investigations will be performed in order to obtain high-performance multi-frequency results, also when the measurements acquisitions are dynamic, to fit actual production lines at the expected velocity.

Acknowledgment

This publication is part of the project PNRR-NGEU which has received funding from the MUR – DM 117/2023. This research was supported in part by the project PON Research and Innovation, "Microwave Imaging and Detection powered by Artificial Intelligence for Medical and Industrial Applications (DM 1062/21)," and in part by the PRIN project "BEST-Food, Broadband Electromagnetic Sensing Technologies for Food Quality and Security Assessment"; both projects are funded by the Italian Ministry of University and Research (MUR). The research was supported also by the project "INSIGHT-FOOD – An innovative microwave sensing system for the evaluation and monitoring of food quality and safety", funded by the Italian Ministry of Foreign Affairs and International Cooperation (MAECI).

References

[1] E. Commission, D.-G. for Health, and F. Safety, *RASFF annual report 2018*. Publications Office, 2019.

[2] J. A. Tobon Vasquez, R. Scapaticci, G. Turvani, M. Ricci, L. Farina, A. Litman, M. R. Casu, L. Crocco, and F. Vipiana, "Noninvasive inline food inspection via microwave imaging technology: An application example in the food industry," *IEEE Antennas and Propagation Magazine*, vol. 62, no. 5, pp. 18–32, 2020.

[3] M. Ricci, J. A. T. Vasquez, R. Scapaticci, L. Crocco, and F. Vipiana, "Multi-antenna system for in-line food imaging at microwave frequencies," *IEEE Transactions on Antennas and Propagation*, vol. 70, no. 8, p. 7094 – 7105, 2022.

[4] M. Ricci, J. A. T. Vasquez, R. Scapaticci, G. Turvani, M. R. Casu, L. Crocco, and F. Vipiana, "Preliminary in-line microwave imaging experimental assessment for food contamination monitoring," in *2023 17th European Conference on Antennas and Propagation (EuCAP)*, 2023.

[5] A. Darwish, M. Ricci, J. A. Tobon Vasquez, C. Migliaccio, and F. Vipiana, "Near-field microwave sensing technology enhanced with machine learning for the non-destructive evaluation of packaged food and beverage products," *Scientific Reports*, vol. 14, no. 1, 2024.

[6] D. O. Rodriguez-Duarte, J. A. T. Vasquez, R. Scapaticci, L. Crocco, and F. Vipiana, "Assessing a microwave imaging system for brain stroke monitoring via high fidelity numerical modelling," *IEEE Journal of Electromagnetics, RF and Microwaves in Medicine and Biology*, vol. 5, no. 3, pp. 238–245, 2021.

[7] S. K. Palaniswamy, M. Kanagasabai, S. Arun Kumar, M. G. N. Alsath, S. Velan, and J. K. Pakkathillam, "Super wideband printed monopole antenna for ultra wideband applications," *International Journal of Microwave and Wireless Technologies*, vol. 9, no. 1, p. 133–141, 2017.

[8] "M9804A PXI Vector Network Analyzer, 9 kHz to 20 GHz." Available at https://www.keysight.com/us/en/assets/3119-1014/data-sheets/5992-3596.pdf.

[9] "N1500a materials measurement suite." Available at https://www.keysight.com/it/en/product/N1500A/materials- measurement- suite.html.